Development of a large-eddy simulation open channel code

J. Shi, T.G. Thomas and J.J.R. Williams
Turbulence Unit, Queen Mary and Westfield College, University of London, London, UK

Keywords *Codes, Eddy current, Finite differences, Turbulence*

Abstract *Describes further development of a 3D finite difference code written to model turbulent flows in an open channel with a moving free surface. The code has been developed so that the computational domain can have side-walls and/or periodic directions and that the flow may also be buoyancy driven. Either a full simulation or large eddy simulation (LES) of the turbulence can be performed. Results are presented of a simulation of periodic streamwise flow in an open channel with parallel side-walls and also of a thermal jet into an open tank. Both simulations were carried out on a UNIX workstation using resolutions that enable the results to be viewed within an "engineering context". The LES application demands numerical approximations which conserve mass, momentum and total energy with high precision, and which permits wave motion with very little numerical dispersion or dissipation. The free surface is tracked using a split-merge technique which combines the volume of fluid (VOF) and height function methods in a way that is conservative.*

Introduction

The structure of turbulence at a free liquid surface and the physical processes involved there have an important practical role in the dispersion of thermal discharges and pollutants in rivers and coastal waters as well as being interesting in their own right. Our understanding of these processes is limited owing to the experimental difficulties of obtaining reliable and detailed turbulence measurements close to a moving surface and, also, due to the lack of a satisfactory numerical surface boundary condition for k-ε or algebraic models.

A reliable code must be able to model the turbulent, buoyancy and free-surface effects accurately and it is now possible to do this through the use of supercomputers in which the Navier-Stokes equations are integrated directly without making any modelling assumptions. However, this approach, which is known as full simulation or direction numerical simulation (DNS), is feasible only for flows at relatively low Reynolds number and in regions of simple shape. The drawback to the method is that the computational effort required to model flows of engineering importance (and hence large Reynolds numbers) lies beyond our reach for the foreseeable future.

An alternative approach closely related to DNS is large eddy simulation (LES) in which only the large eddies or grid scales are represented explicitly on a finite difference grid. The interactions of these grid scales with the unrepresented small eddies or sub-grid scales (SGS) are represented by a sub-grid model (SGM). This method is therefore dependent on a model, but experience has shown that the sensitivity of the results to the details of the

International Journal of Numerical Methods for Heat & Fluid Flow, Vol. 9 No. 1, 1999, pp. 6-17,

model is quite weak which contrasts with the much greater sensitivity of k-ε and algebraic stress models of turbulence to their model constants.

Apart from surface tension (which is disregarded), this code treats the free-surface stress conditions exactly and further details of the code's earlier development can be obtained from Thomas *et al.* (1995).

Numerical method

The basic finite difference procedures used in the code are based on the QMW finite difference closed channel code ECCLES (Gavrilakis *et al.,* 1986) which uses a conventional staggered grid and is conservative. In this code, the 3D Navier-Stokes equations are solved using second order central differences with the velocities (without the pressure terms) being advanced by the Adams-Bashforth technique. A Poisson equation is then solved for the pressure and the advanced velocities are corrected by inclusion of the pressure gradients in order to conserve mass. However, both in ECCLES and in our earlier free-surface code, the flow must be periodic in the x and y directions and solid walls are only allowed in the z direction. The object of the present work was, therefore, to incorporate side-walls and also a buoyancy term. The free-surface treatment remains the same in that because LES simulations have long integration times and it is necessary to conserve energy in the finite sense (as well as that for wave propagation), the authors felt that it was not possible to use the more established techniques such as MAC, VOF or mapping of the domain. The authors are not aware of any other free-surface LES codes that, in turn, allow the free-surface to freely deform, treat the free-surface stress terms exactly and are able to model channels with side-walls and buoyancy terms. Consequently, it is the first time that the LES technique has been applied to the applications reported in this paper.

Governing equations

Cartesian co-ordinates (x, y, z) are used in which x and y are aligned with the channel walls and z is normal to the channel bed. The flow is maintained by gravity $\mathbf{g} = (g_x, g_y, g_z)$ and we assume that there is no externally applied surface pressure. The velocity u and pressure p satisfy the Navier-Stokes equations with a Boussinesq buoyancy term:

$$\partial \mathbf{u}/\partial t + \mathbf{u}.\nabla \mathbf{u} = -\nabla p + \nabla.\tau + g_Z\beta(T_o - T_a)Q + \mathbf{g} \quad (1)$$

$$\partial Q/\partial t + \mathbf{u}.\nabla Q = a\nabla^2 Q \quad (2)$$

$$\nabla.\mathbf{u} = 0 \quad (3)$$

where τ denotes the viscous and subgrid stress, β is the coefficient of thermal expansion, a is the thermometric conductivity and $Q = (T - T_a)/(T_0 - T_a)$. T is the fluid temperature, T_0 is the temperature of the inflow and T_a is the ambient temperature.

The elevation of the free surface is given in terms of a single-valued height function h, such that:

$$z = h(x,y,t), \tag{4}$$

$$|dh/dx| \leq \Delta z/\Delta x \text{ and } |dh/dy| \leq \Delta z/\Delta y. \tag{5}$$

The maximum slope restriction – based on finite difference mesh size Δx, Δy, Δz, is imposed because it allows a much simplified surface locator. The single-valued nature of h excludes wave breaking. The kinematic free surface boundary condition is given by:

$$dh/dt = (\mathbf{u}.\mathbf{n})\sqrt{S}, \tag{6}$$

$$S = 1 + (dh/dx)^2 + (dh/dy)^2, \tag{7}$$

$$\mathbf{n} = (-dh/dx, -dh/dy, 1)\sqrt{S}. \tag{8}$$

Equation (6) states that the rate of change of surface elevation is proportional to the flux of fluid over the surface; it can be written in the more usual convective form by eliminating ($u.n$). The quantity S is simply the ratio of sloping surface area to vertically projected surface area, and n denotes the surface unit normal vector. The dynamic free surface condition is:

$$\mathbf{n}.(\tau - p\mathbf{I}) = 0 \tag{9}$$

which states that both the total normal stress (including the viscous component) and the tangential stress must be zero; **I** denotes the unit tensor.

Side wall code development

The ability to model side walls was added to the code so that the flow domain could have the option of:

(1) walls on all four sides;

(2) walls on two opposite sides only with periodic flow conditions in the other direction; and

(3) periodic flow in both horizontal directions.

A choice of free and no-slip boundary conditions are allowed where, in the case of a no-slip condition, a modified form of the Werner and Wengle (1993) power-law boundary condition was utilised which relates the instantaneous local stress and to the nearest wall cell velocity: $u^+ = A(z^+)^{1/7}$. The coefficient A was altered from its original value of 8.3 to 8.45 so that the velocities at the first grid points always fell on the open channel log-law profiles (Nezu and Rodi, 1986). In using this technique the need to determine average streamwise velocities for the nearest wall cells in partially full cells near the free surface (as would be

required for the Schumann (1975) technique) was avoided. Other modifications included the addition of outflow windows to the walls in order to extract a constant inflow per unit length of wall and a circular jet inflow through the bed.

Side-wall channel simulation

Flow in an open channel with side walls is characterised by the occurrence of turbulence-driven secondary currents that are responsible for the maximum velocity to occur below the free surface and for the occurrence of streamwise ridges and troughs on a movable river bed. These secondary currents move low streamwise momentum fluid from the sides to the centre of the channel and high momentum fluid from the free surface towards the bed. This movement, in turn, causes a wavy distribution in the wall and bed shear stresses. The production, dissipation and transport of mean streamwise vorticity can be shown to be dependent on the distribution of the secondary Reynolds stresses around the channel sides. In addition, there is also a considerable difference in the flow pattern between the secondary currents in closed and open channels caused by the existence of the free surface, which dampens the vertical turbulent fluctuations. In order, therefore, to realistically simulate flow in an open channel with side walls a code must also be able to simulate the secondary motions which, in turn, means being able to numerically model accurately the turbulent stresses around the sides and at the free-surface.

The time averaged streamwise vorticity equation can be obtained by cross-differentiating the y and z components of equation (1). If we consider only fully developed flow, i.e. all gradients with respect to x are zero, then this equation reduces to:

$$(\mathbf{U}.\nabla)\,\Omega_x = \partial^2(\overline{w^2} - \overline{v^2})/\partial y\partial z - (\partial^2/\partial z^2 - \partial^2/\partial y^2)\,\overline{vw} + \nu\nabla^2\Omega_x \qquad (10)$$

where $\Omega_x = \partial W/\partial y - \partial V/\partial z$ and ν is the kinematic viscosity. (U, V, W) and (u, v, w) are the time averaged and fluctuating velocities respectively.

According to Demuren and Rodi (1984), the first two terms on the right hand side of equation (8) are an order of magnitude greater than the other terms. Gessner and Jones (1965) first found that both of these terms contribute to the production of secondary flow whereas Perkins (1970) argued that the secondary flow is generated by the first term on the right hand side and the second acts like a transport term. The last term, which is the viscous dissipation, is only significant near the walls and corners.

Computational domain

In order to check the code's ability to model free-surface open channel flow and also to investigate the resolution required for "engineering purposes", a relatively coarse simulation of turbulent incompressible flow down an open channel was carried out. The vertical gravity component, g_z, was set to 1,700 to give a Froude number $(u_{mean}/(g_z H)^{1/2}) = 0.54$. The flow was maintained with mean bed and side wall stress $\tau_{mean} = \rho u_\tau^2$ where u_τ denotes the characteristic shear velocity $= (\propto g_z R)^{1/2}$, $\propto$ is the channel slope relative to the x axis, ρ is the

density and R the hydraulic radius. The two characteristic lengths for this flow are the depth H and the viscous length ν/u_τ. The ratio $u_\tau H/\nu$ is denoted Re^+ and is set equal to 2,200 to match experiments performed by Nezu and Rodi (1985) (hereafter denoted NR). The computed Reynolds number, R_e, (defined as $4RU_{mean}/\nu$) was 90,400, which compares with the NR valve of R_e = 97,000. A computational domain of box size, $A \times B \times H = 6 \times 2 \times 1$, was used giving an aspect ratio $B/H = 2$. A moderately coarse resolution was used $32 \times 32 \times 16$ points in the streamwise, cross-stream and vertical directions respectively giving mesh sizes in wall units of $\Delta x^+ = 450$ and $\Delta y^+ = \Delta z^+ = 150$. Streamwise correlations for all three velocities were calculated and were shown to be very near zero for a box length of $A = 6H$. The Smagorinsky sub-grid scale model (Smagorinsky, 1963) was used with the constant $C_0 = 0.1$.

The total run time for the simulation, which was carried out on a Silicon Graphics Indigo 2 workstation, was approximately 200 hours. This is about three times greater than that required for turbulence to fully develop in a similar flow configuration without side-walls and is due to the very large amount of time necessary for the secondary currents to fully develop. A doubling of resolution would increase the overall run time by a factor of 16.

Numerical results

Mean streamwise velocity

Figures 1(a) and (b) show the computed and NR measured mean streamwise velocity distribution across the channel section. Both the maximum velocity dip near the free surface and typical corner flow contours owing to turbulence driven secondary currents can clearly be seen.

The computed non-dimensional maximum mean velocity, u_m/u_τ, is 25, which compares exactly with that obtained by NR while the computed total non-dimensional discharge is 43.0, which compares favourably with the experimental value of 44.6. However, the location of the maximum velocity, z_{max}, occurs at approximately $z_{max}/H = 0.75$, rather than at 0.63 obtained by NR. In comparing simulated discharges and shear stresses (see below) with those measured, it is worth noting that NR determined the boundary shear stresses by fitting a log profile to measured velocities around the channel periphery using a least squares procedure and not by direct measurement. It was the sum of these local values that gave the published average boundary shear stress and Re^+, which was then used by the authors in the simulation. Thus any errors arising from this procedure (which would be greater near the corners where the log-law velocity profile is no longer applicable) would mean that the published average boundary shear stress would also be in error to some unknown degree.

Secondary currents

Figures 2(a) and (b) show measured (by NR) and computed long time averaged secondary current velocity vectors respectively. It can be seen that the LES results capture the two main free-surface and bottom vortices together with the much smaller anti-clockwise vortex occurring at the junction of wall and free-

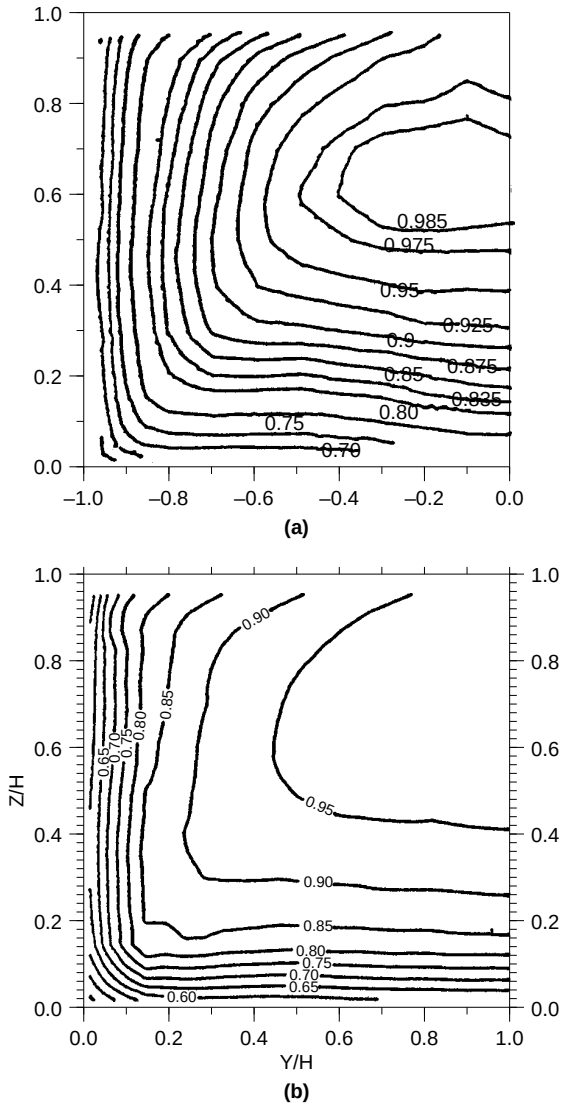

Figure 1. Isolines of mean streamwise velocity; (a) measured; (b) computed

surface. In general, there is good comparison between the two sets of results but the computed bottom vortex is, to some extent, stronger that the measured one while the computed top vortex is somewhat weaker than that measured. The relatively weak top vortex, in particular, could explain the computed high positioning of the maximum centreline velocity.

Mean bed and wall shear stresses

The computed and measured bed and side wall shear stresses normalised by the averaged bed and side wall stresses, τ_{mean}, is shown in Figure 3. Both the

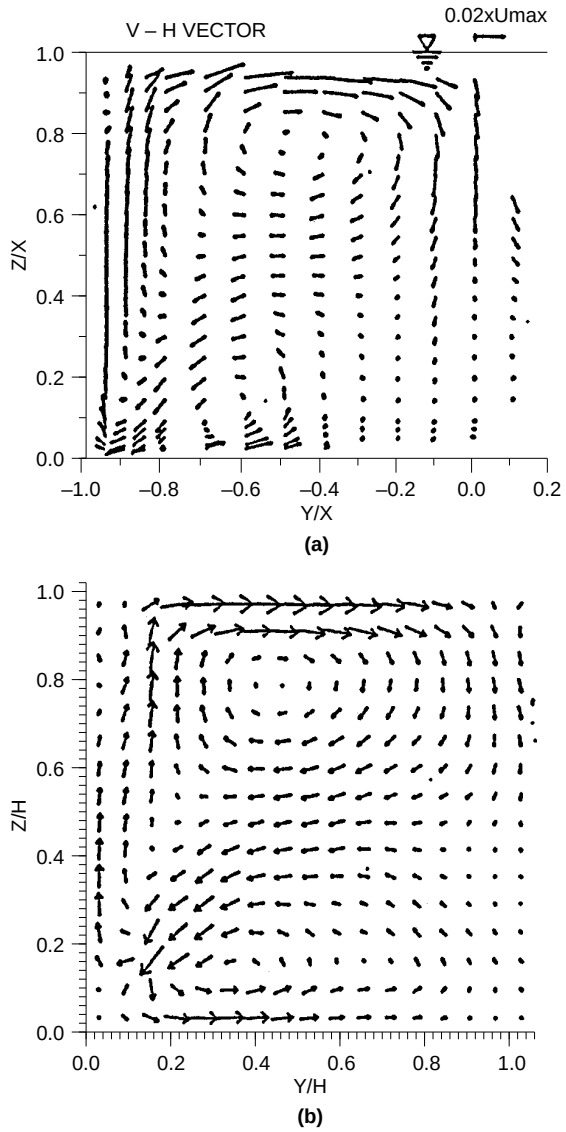

Figure 2.
Secondary currents:
(a) measured; and
(b) computed

computed side wall stress (Figure 3(a)) and bed stress (Figure 3(b)) are, generally, in good agreement with those measured, with the largest differences occurring at the corners and in the centre of the bed of the channel. The differences in the corners could be due to the inapplicability of the log-law used in these locations to determine the measured shear stress while the channel centre differences could be due to the relatively weaker than measured streamwise vortices not drawing down the correct amount of secondary flow, which would have increased the local value of the bed shear stress.

Production of secondary currents

Figures 4(a) and (b) show contours of the experimental and computed values of the streamwise vorticity production term $(\overline{v^2} - \overline{w^2})/U_{max}^2$. As there are no NR values available, comparisons have been made with the experiments of Tominaga *et al.* (1989) who carried out similar tests to NR but at a R_e = 73,100. It can be seen that the results agree reasonably well with each other in the channel centre but that the differences become greater near the walls. While it must be difficult to measure these turbulent terms accurately, it does seem that insufficient resolution has been used in the numerical simulation near the walls where the streamwise vorticity is produced.

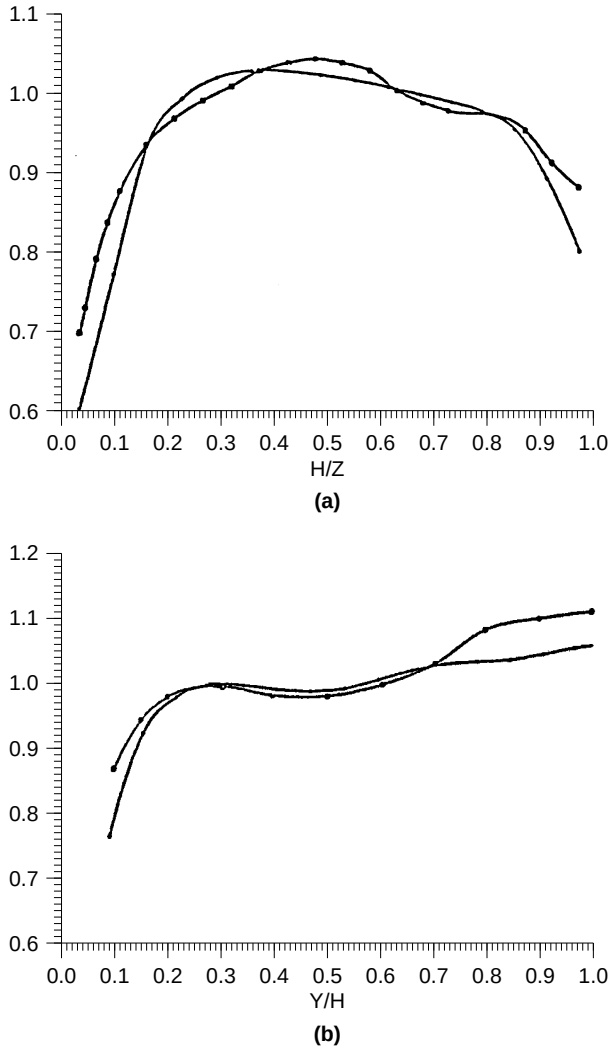

Figure 3. Comparison of measured, (NR), and computed, •, wall and bed stresses

Thermal plume

The flow characteristics of a vertical turbulent buoyant jet discharging into a shallow fluid are dependent on: the initial momentum of the jet, its initial temperature relative to the ambient temperature of the receiving fluid, the jet diameter and the depth of the receiving fluid. The modelling of such a problem therefore presents a good test of the free-surface codes ability to model:

(1) a transportable scalar (temperature in this case);

(2) buoyancy effects; and

(3) the interaction of the jet with the free-surface.

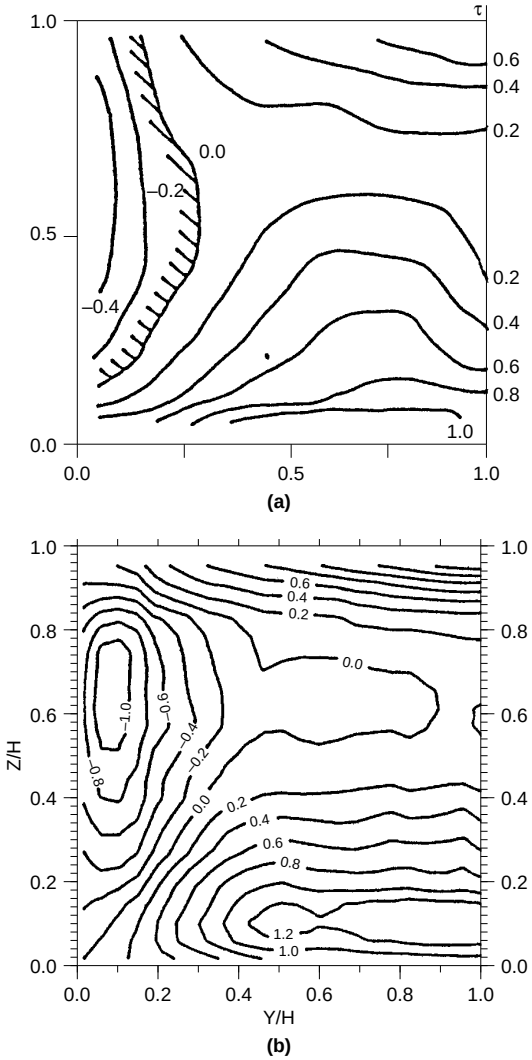

Figure 4.
Isolines of $(\overline{v^2} - \overline{w^2})/Umax2 \times 10^3$: (a) measured; and (b) computed

A fundamental concern is the discharge stability of the jet: it rises from the bottom of the shallow fluid towards the surface and, after impingement, spreads horizontally. By definition, if a simple buoyant stratified flow spreads along the bounding surface, it is said that the resulting spreading motion is stable. Otherwise, it is not stable if a recirculating eddy is formed over the entire layer depth (see Figures 5 (a) and (b)). The two parameters governing the flow behaviour are the ratio of depth to discharge orifice diameter, H/D, and the densimetric Froude number, $F_0 = u_0/(gD\Delta\rho_0/\rho_a,)^{1/2}$, in which $\Delta\rho_0/\rho_a = (\rho_0 - \rho_a)/\rho_a$. u_0 is the discharge velocity of the jet with density ρ_0, ρ_a is the density of the receiving fluid and g is the acceleration due to gravity. F_0 is therefore the ratio of inertial to buoyancy force.

A simulation of a stable configuration was performed to match the experimental work of Lee and Jirka (1981) in which the box size was $3H \times 6H \times H$ with the depth $H = 1$ and the jet placed in the box centre of the long side and having a diameter = $0.25H$ ($H/D = 4$). The flow conditions were set so that they matched the experimental work where the Reynolds number (based on outflow velocity, jet diameter and viscosity) was 6,800 and the temperature of the jet was 12.2°C greater than that of the receiving water giving $F_0 = 8.2$. The number of grid points used in the horizontal and vertical directions per unit length (i.e. H) was 32 with uniform spacing. This gave eight points across the jet diameter although to fully resolve the jet would require a much greater resolution than this (Akselvoll and Moin, 1996). The total run time on a Silicon Graphics Indigo 2 workstation was approximately 60 hours and, again, a doubling of resolution would increase this by a factor of 16.

Figure 6 shows a velocity vector plot obtained from averaged radial and vertical velocities taken at approximately the time when the jet has first reached

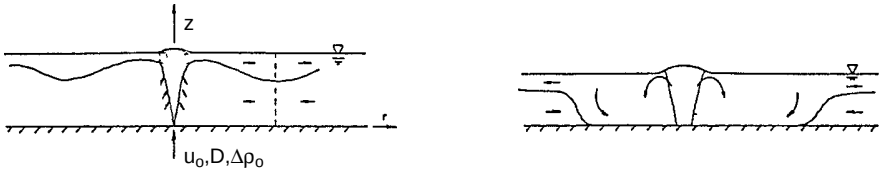

(a) stable discharge **(b)** unstable discharge

Figure 5. Vertical round buoyant discharge in shallow water

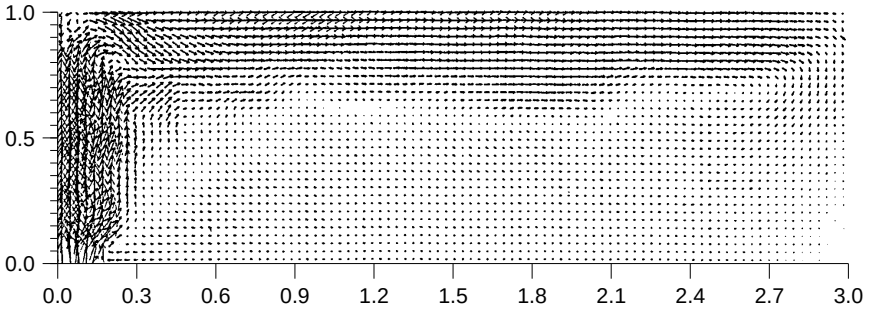

Figure 6. Calculated radially averaged velocity vectors

the outer walls. It can be seen that a narrow jet rises to the surface where it then spreads out smoothly to form an internal hydraulic jump. No detailed experimental data are available to compare with these results but Figure 7 shows a diagrammatic plot of the expected temperature interface for a stable internal hydraulic jump taken from Lee and Jirka (1981) for a H/D of 11 and a densimetric Froude number, F_0, = 46. Figure 8 shows a contour plot of the averaged computed flow temperatures taken at the same time as Figure 6 and it can be seen that a stable jump does appear to be evident.

No special treatment of the temperature transport terms was used (i.e. central differences were used throughout) except that cell temperatures were clipped if they exceeded 1 or fell below zero. In order to prevent an artificial circulation occurring at the base of the jet owing to the use of an Adams-Bashforth time stepping scheme (which is mildly unstable), the molecular viscosity had to be increased slightly. No sub-grid scale model was used.

Conclusions

Turbulence-driven secondary motions in an open channel at ratio B/H = 2 have been simulated using an LES code that allows the free surface to freely deform. A relatively large Reynolds number and coarse mesh was used in the simulation, producing results that compare favourably with those measured but indicate that a higher degree of resolution may be necessary in order to reproduce more accurately the streamwise vorticity production term. It is the correct simulation of this term which drives the secondary currents and produces the characteristic velocity dip in narrow open channels.

A successful simulation was carried out of a thermal plume and internal hydraulic jump in a shallow body of water. The code was able to reproduce the essential features of a laboratory experiment without any special treatment of the temperature transport terms.

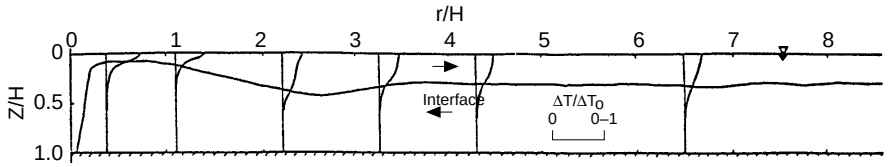

Figure 7.
Diagrammatic plot of the temperature interface for F_0, = 46 and H/D = 11

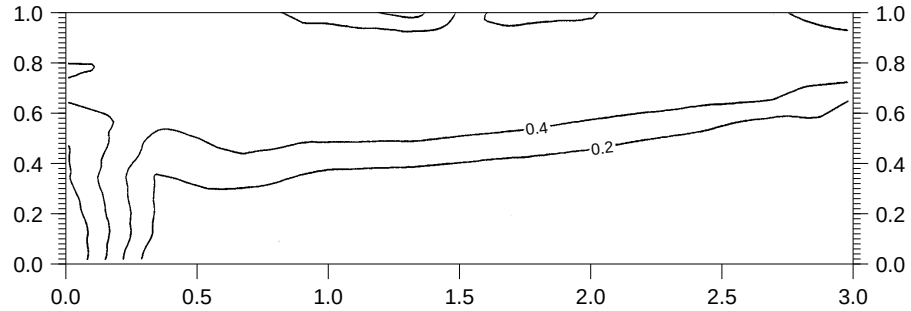

Figure 8.
Calculated radially averaged temperature contours

References

Akselvoll, K. and Moin, P. (1996), "Large-eddy simulation of turbulent cofined coannular jets", *J. Fluid Mech.,* Vol. 315, pp. 387-411.

Demuren, A.O. and Rodi, W. (1984), "Calculation of turbulence-driven secondary motion in non-circular ducts", *J. Fluid Mech.,* Vol. 140, pp. 189-222.

Gavrilakis, S., Tsai, H.M., Voke, P.R. and Leslie, D.C. (1986), in Schumann, U. and Friedrich, R. (Eds), *Notes on Numerical Fluid Mechanics,* Vol. 15, Vieweg, Braunschweig, p. 15.

Gessner, B.F. and Jones, J.B. (1965), "On some aspects of fully developed turbulent flow in rectangular channels", *J. Fluid Mech*., Vol. 23, p. 689.

Lee, H.W. and Jirka, M. (1981), "Vertical round buoyant jet in shallow water", *J. Hydraulics Div.,* ASCE, HY12, Vol. 107, pp. 1651-75.

Nezu, I. and Rodi, W. (1985), "Experimental study on secondary currents in open channel flow", *Proceedings of 21st IAHR Congress*, Melbourne, Vol. 2, pp. 115-19.

Nezu, I. and Rodi, W. (1986), "Open channel flow measurements with a laser doppler anemometer", *J. Hyd. Engng*, ASCE, Vol. 112 No. 5, pp. 335-54.

Perkins, H.J. (1970), "The formation of streamwise vorticity in turbulent flow", *J. Fluid Mech*., Vol. 44, p. 721.

Schumann, U. (1975), "Subgrid-scale model for finite difference simulations of turbulent flows in plane channels and annuli", *J. Comp. Phys.,* Vol. 18, pp. 376-404.

Smagorinsky, J. (1963), "General circulation experiments with the primitive equations. I. The basic experiment", *Mon. Weather Rev.,* Vol. 91, pp. 99-164.

Thomas, T.G., Leslie, D.C. and Williams, J.J.R. (1995), "Free surface simulations using a conservative 3D code", *J. Comp. Phys*., Vol. 116, pp. 52-68.

Tominaga, A., Nezu, I., Ezakl, K. and Nakagawa, H. (1989), "Three-dimensional turbulent structure in straight open channel flows", *J. Hydraulic Research*, Vol. 27 No. 1.

Werner, H. and Wengle, H. (1993), "Large-eddy simulation of turbulent flow over and around a cube in a plane channel", *TSF8*, Springer-Verlag, Berlin.